Received: 8 December 2023 | Accepted: 15 December 2023

DOI: 10.1002/ppap.202300226

RESEARCH ARTICLE

PLASMA PROCESSES AND POLYMERS

Ion chemistry and ionic thin film deposition from HMDS-photochemistry induced by VUV-radiation from an atmospheric plasma

Tristan Winzer[1] | **Jan Benedikt**[1,2]

[1]Institute of Experimental and Applied Physics, Kiel University, Kiel, Germany

[2]Kiel Nano, Surface and Interface Science KiNSIS, Kiel University, Kiel, Germany

Correspondence
Tristan Winzer and Jan Benedikt, Institute of Experimental and Applied Physics, Leibnizstr. 19, 24118 Kiel, Germany.
Email: winzer@physik.uni-kiel.de and benedikt@physik.uni-kiel.de

Funding information
Deutsche Forschungsgemeinschaft; German Research Association, Grant/Award Number: BE 4349/7-1

Abstract

Injection of precursor molecules into a plasma often results in particle generation or deposition in the source, compromising film quality and plasma operation. We present here a study of ion chemistry and ionic film deposition from hexamethyldisilane (HMDS) using a novel device utilizing vacuum ultraviolet (VUV)-radiation from a remote atmospheric plasma. Infrared spectroscopy showed that SiO_2-like films were obtained at the lowest admixture, where impurities are more important and VUV-photons reach the substrate, while only slightly oxidized films were deposited at high admixtures. Photoionization mainly forms the monomer ion due to collisional stabilization and possibly slow polymerization reactions as found by ion mass spectrometry. The more detailed photochemistry of HMDS-related ions is discussed based on mass spectra for different admixtures.

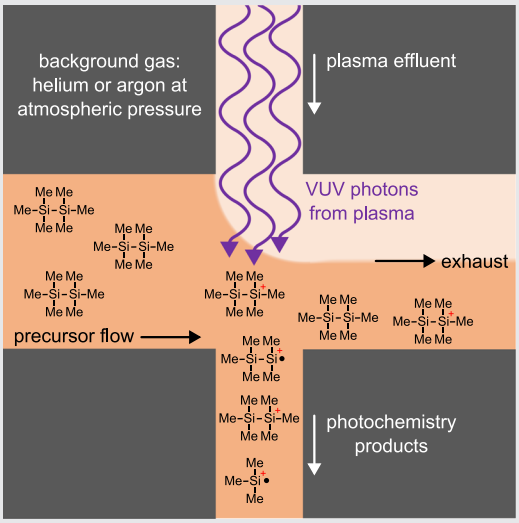

KEYWORDS
atmospheric-pressure plasma, capillary jet, FTIR, hexamethyldisilane, ion mass spectrometry, photochemistry, thin-film deposition, VUV photons

1 | INTRODUCTION

$SiC_xH_yO_z$ thin films have a variety of unique characteristics, depending on their composition, deposition process, and the resulting film properties. They can be used as a low-k dielectrics,[1] protective coatings as silicone-carbide (SiC), or in their extreme cases as barrier coatings in the form of silicon-dioxide (SiO_2).[2] Based on their properties, SiC coatings on polymers could provide a protective layer against mechanical damage and UV-radiation-induced degradation.[3] Successful deposition of SiC from a combination of SiH_4 and C_3H_8 in H_2 using conventional chemical-vapor-deposition (CVD) and plasma-enhanced CVD (PE-CVD) has been reported in the literature (see e.g.,[4–7]). However, the use of SiH_4 and H_2 necessitates extensive safety precautions, that can be avoided by using more stable single-source organosilicon precursors that possess both the necessary silicon and carbon atoms in one molecule. Among these precursors, hexamethyldisilane (HMDS, $Me_3SiSiMe_3$) plays a special role due to its chemical inertness under ambient conditions and weak Si–Si bond.[8] This molecular structure makes it prone to decomposition even under comparably mild conditions, lowering the necessary temperature for the CVD process.[9–12] Still, substrate temperatures for conventional CVD from HMDS need to be around 1000°C or higher, making this process unsuitable for film deposition, for example, on heat-sensitive polymer surfaces. Therefore, several techniques for thin-film deposition have been developed to overcome this challenge including hot-wire CVD (HW-CVD),[13] ion beam deposition [14–16], and PE-CVD at low pressures.[17–20]

Admixing reactive gases into plasma creates several challenges such as deposition inside the source or formation of negative ions, especially in the case of electronegative gases such as SiH_4 or C_2H_2, with subsequent particle formation, which can be incorporated as defects in the deposited film.[20,21] To overcome the drawback of particle formation, extensive work has been carried out on expanding thermal plasmas with silane (SiH_4) for deposition of amorphous hydrogenated silicon (a-Si:H) films[22–24] and acetylene (C_2H_2) for amorphous hydrogenated carbon (a-C:H) film deposition,[25–29] in which the electrons stay cold, with energies below those needed for formation of negative ion resonances, and negative ion formation is thus avoided.[30,31] Another proposed technique for defect-free thin-film deposition of amorphous hydrogenated silicon-carbon (a-Si:C:H) from organosilicon precursors is remote-hydrogen-plasma CVD (RHP-CVD). Atomic hydrogen is produced in a low-pressure hydrogen plasma and transported into the remote section, where it interacts with the precursor inducing fragmentation and subsequent deposition.[32–41]

Atmospheric-pressure PE-CVD can enable continuous deposition on vacuum-sensitive surfaces,[42] but the deposition of defect-free films is even more of a challenge at atmospheric pressure, where collision rates are substantially higher.[43] This is supported by works on PE-CVD, which found an increasing particle size with higher pressure in PE-CVD.[20,21] Nanoparticles have even been synthesized from HMDS using atmospheric-pressure CVD without the use of a plasma.[44] To avoid particle formation and deposition inside the source during atmospheric-pressure PE-CVD from organosilicon precursors by reducing the residence time of reactive species in the plasma, sources with on-axis precursor injection[45,46] and single-filament discharges have been proposed.[47]

First experiments on the decomposition of HMDS using photolysis have shown the deposition of films on the walls of the irradiance cell[48] or detector electrodes[49] followed by a study of HMDS photochemistry in the presence of a polymer surface.[50] Decomposition of HMDS with the following deposition can, therefore, be initiated solely by vacuum ultraviolet (VUV)-radiation. Atmospheric-pressure plasmas in pure helium or argon are efficient sources of this radiation down to 60 nm (helium case) from noble gas excimers.[51,52] Especially the wavelength region below 120 nm is not easily available due to the cut-off wavelength of typically used magnesium or lithium fluoride windows. The highly energetic photons can be utilized to remotely initiate photochemistry, including ionization, in precursor gases. However, VUV-radiation is absorbed by air and the separation of plasma species and radiation at atmospheric pressure is challenging.[53]

In this work, we report on a newly developed atmospheric pressure source for thin-film deposition based on photochemistry induced by VUV-radiation generated by an atmospheric plasma. We used pure argon or helium as a plasma feed gas and HMDS as a model precursor. Analysis of the photochemistry was performed by positive ion mass spectrometry and deposited films were analyzed using Fourier-transform infrared (FTIR) spectroscopy. Based on the observed ions, we propose possible reaction pathways.

2 | EXPERIMENTAL SETUP

2.1 | Capillary-Photon-Jet

The so-called Capillary-Photon-Jet (CPJ) is based on the Photon-Jet[53] and the Capillary-Jet.[54] It features the

same excitation scheme as the Capillary-Jet with the plasma being ignited inside a borosilicate capillary (VitroCom) with a square cross-section of 1 mm by 1 mm and a wall thickness of 0.2 mm acting as a dielectric in front of the electrodes. This leads to an electrode gap of 1.4 mm with an electrode length of 4 cm. One electrode is driven by a sinusoidal radio-frequency (RF) voltage with a frequency of 13.56 MHz via an RF generator (Coaxial Power Systems RFG-150-13) and a matching network (Coaxial Power Systems MMN-150-13), while the other electrode is grounded. Due to the cross-field geometry with electric field perpendicular to the gas flow, the plasma is closely confined between electrodes. In contrast to our previous work on the Capillary-Jet, neither voltage nor current was measured at the CPJ due to the limitations of the setup. Comparable operating conditions for different measurement series with the same plasma gas were achieved by always using the same combination of cables, generator, and matchbox with the same settings at the matchbox and generator. If not stated otherwise, the generator power was set to 10 W for all measurements presented in this work. As only pure argon (99.9999%) or helium (99.999%) was used as a feed gas for the plasma with no other gases admixed, these precautions are sufficient to assure the same operating conditions. Gas flows were adjusted using mass-flow-controllers (MKS G-Series). The generator power translates to a plasma power below 1 W leading to effluent gas temperatures slightly above ambient temperature,[54] hence avoiding thermal decomposition of the precursor.

A sketch of the CPJ is shown in Figure 1. One end of the capillary is glued into a stainless-steel block housing the crossing gas channel using vacuum compatible glue. The distance between the plasma and the crossing section is approximately 10 mm. VUV-photons produced in the plasma travel this distance through the noble gas atmosphere. Helium or argon resonance lines are expected to be fully reabsorbed by the noble gas atmosphere on the way to the intersection, which leads to the radiation being dominated solely by the excimer continua with possible lines from oxygen impurities as shown in Figure 2 in a wavelength range from 60 to 150 nm. The data in Figure 2 has been obtained with the Capillary-Jet for pure argon or helium (each with 500 sccm, 4 W plasma power) using the setup introduced by Golda et al.[52] This figure also includes the photoionization thresholds of HMDS, argon, and the most common feed gas impurities N_2, O_2 and H_2O (ionization thresholds of 15.58,[55] 12.07,[56] and 12.62 eV,[57] respectively). Based on the emission spectra, we expect selective ionization of HMDS by the photons from the argon plasma, while ionized impurities could contribute to the

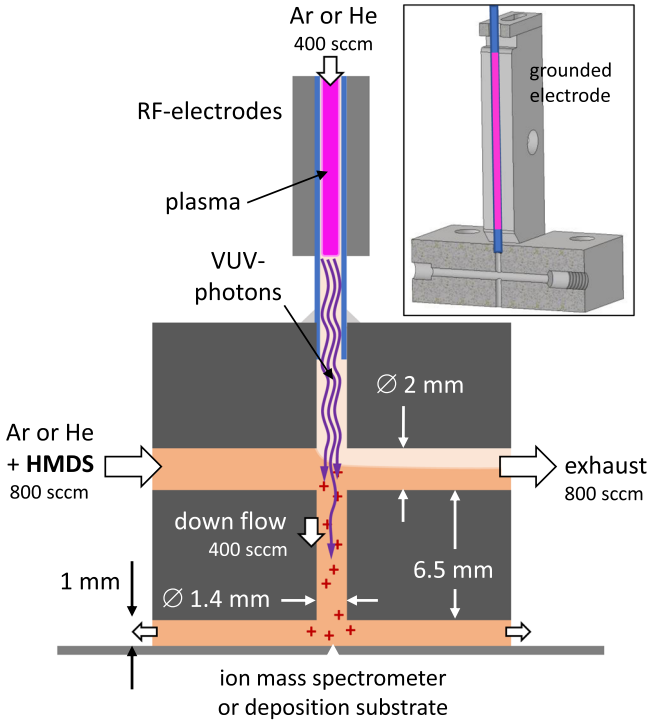

FIGURE 1 Schematic setup of the Capillary-Photon-Jet. The plasma feed gas is supplied from the top, while the precursor is admixed to the crossing gas channel from the side. For efficient separation of plasma species and photochemistry products, the crossing flow is twice as high as the gas flow through the plasma, while also the cross-sectional area of the crossing channel is a factor of two larger. The inset shows a three-dimensional (3D)-cross-section of the real jet machined from stainless steel.

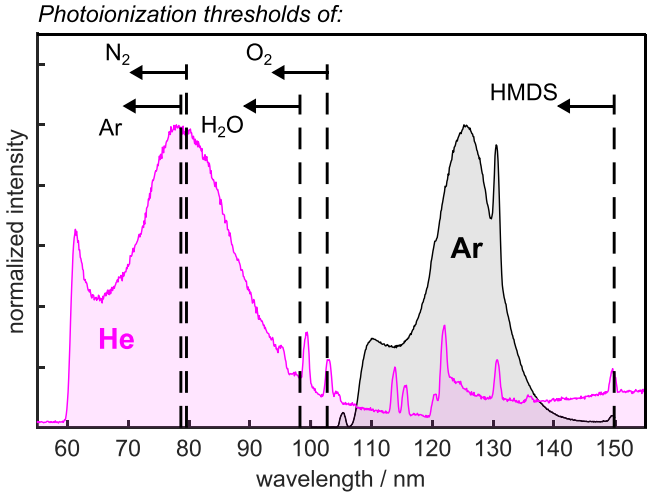

FIGURE 2 Emission spectra between 60 and 150 nm from pure helium and pure argon plasma in the Capillary-Jet with additional lines from impurities in the feed gas. The spectra have been normalized to the maximum intensity of the excimer emission continua. The dashed lines indicate the photoionization thresholds of hexamethyldisilane (HMDS), argon, and common gas impurities.

HMDS photochemistry in the helium plasma radiation case.

The diameter of the vertical gas channel is 1.4 mm to fit the diagonal width of the capillary, while the diameter of the crossing channel is 2 mm. This leads to the crossing channel having approximately twice the cross-sectional area as the vertical channel, which is necessary for the effective separation of plasma-generated species and photochemistry products. Another requirement for this separation is the ratio of gas flows through both channels being 2-to-1 with the higher gas flow through the horizontal channel. If not explicitly mentioned, gas flows used in this work were 400 sccm of argon or helium through the plasma channel and 800 sccm of argon or helium with 100–2000 ppm HMDS through the crossing channel. The exhaust gas flow was adjusted to be 800 sccm, so photochemistry products were transported 6.5 mm to the exit of the device in a downwards directed gas flow of 400 sccm. This leads to a transfer time of 2 ms needed for full replacement of the precursor in this gas channel. The source was always positioned 1 mm above the orifice of the ion mass spectrometer or the deposition substrate, so residual gas is transported to the sides and no over-pressure is building up inside the source.

2.2 | Precursor admixture with bubbler

HMDS (97% purity, abcr GmbH) is admixed to the gas flow by bubbling a fraction of the crossing gas flow through a glass bubbler filled with the monomer in the liquid state. The main impurities in the precursor according to the supplier are hexamethyldisiloxane (HMDSO) and dimethyl(trimethylsilylmethyl)silane adding up to 99.9% when combined with the HMDS. The literature suggests that HMDSO is the main impurity by about an order of magnitude.[58,59] Full admixture control is achieved by diluting the HMDS-enriched gas flow afterwards with pure argon or helium. The flow through the bubbler and the diluting gas flow always add up to 800 sccm. As HMDS is liquid at room temperature and its vapor pressure is comparable to water, no additional precautions are necessary for handling or storing the chemical, when the bubbler vessel is sealed airtight. As the temperature of the HMDS in the bubbler depends on the ambient temperature and the temperature of the bubbling gas, its temperature is monitored by using a Type-K thermocouple immersed in the liquid. The thermocouple is connected to a digital thermometer (UNI-T UT320D). Calculation of the HMDS vapor pressure in the bubbler is performed using the formula given in reference.[60] The uncertainty of the admixture is based on the uncertainty of the temperature measurement and the difference of the real ambient pressure to the 101,300 Pa used in the calculation. The former is calculated based on the accuracy of the thermometer (0.5%+1° C) while the latter is estimated with 2000 Pa. In the range of ambient temperature, this leads to an admixture uncertainty of around 8%.

2.3 | Ion mass spectrometer

Sampling of ions from atmospheric pressure is performed using a setup consisting of two differential pumping stages with the second stage housing the mass spectrometer (HIDEN EQP-6). The gas mixture enters the first stage through a 20μ20 μm platinum orifice (Plano GmbH) inserted into a stainless steel plate. The platinum aperture and the stainless steel plate are shaped in a way, that the supersonic expansion due to the pressure difference between atmospheric pressure and the first pumping stage (10^{-2}–2×10^{-2} Pa) is not disturbed. The first stage is evacuated by a turbo-molecular pump (Pfeiffer Vacuum GmbH) in combination with a scroll pump (Edwards Ltd), to achieve a sufficient pressure gradient from atmospheric pressure. After the expansion, the ions are guided into a second orifice with a diameter of 1 mm by a system consisting of four electrostatic ion lenses with individually adjustable potentials. More details on the setup and tuning of the ion lenses can be found in the literature.[61] The second stage is again pumped by a turbo-molecular pump in combination with a membrane pump (Pfeiffer Vacuum GmbH) to the operating pressure of the mass spectrometer (around 10^{-5}Pa). The quadrupole-filter inside the mass spectrometer separates species based on their mass-to-charge ratio. As the species measured in this work are expected to be singly charged, we use atomic mass units when discussing ion mass spectra in this article.

2.4 | Thin film diagnostics

For studying the films deposited from the photochemistry products of HMDS, a silicon wafer was placed under the CPJ as indicated in Figure 1. The deposition time was always 1 h, because of the low deposition rate. Deposited films have a circular shape, as the exit of the CPJ is also circular and the emanating gas flow propagates in all directions. Analysis of the films was conducted less than 5 min after the deposition to minimize the film aging due to oxidation or contamination with impurities. Films were analyzed in transmission using an FTIR-spectrometer (Bruker VERTEX 80v) with a focusing unit. For each spectrum, 50 scans were

averaged with a resolution of 4 cm^{-1} and an aperture of 4 mm. In the first step, a background measurement of a clean silicon wafer was conducted followed by the film measurements with the infrared (IR) beam (diameter 1 mm) at the center of the deposits. The absorption spectra of the films were background- and baseline-corrected in postprocessing.

Additionally, the film thickness has been analyzed by profilometry using a stylus profilometer (Bruker DektakXT). Measurements were taken with a stylus of 2 μm radius and a force of 1 mg in two directions across the deposits.

3 | MEASUREMENT PROCEDURE AND DATA PREPARATION

Before starting a measurement series, the setup and feed gas lines were flushed with 400 sccm argon or helium through the plasma channel, 70 sccm argon or helium through the bubbler and 730 sccm diluting gas flow for 15 min. Afterwards, the plasma was switched on and the gas flows were adjusted to the flows for the first measured admixture. After another 5 min, we assumed stable plasma operating conditions and the measurement was started. In between measurements, we waited another 5 min after changing the HMDS admixture, to assure that all flows are stable. The HMDS temperature was always checked before setting a new admixture and checked again before starting a measurement.

The mass spectrometer and the electrostatic lens system were optimized for the maximum signal of the HMDS ion. As tuning of the mass spectrometer also includes setting a fixed ion energy to the electrostatic ion energy filter, the signals of ions with higher and lower masses will be discriminated, due to the weak dependency of the ion energy on the ion mass.[61] To make sure that all ions are measured at the proper energy, we always recorded several mass spectra in an ion energy range of 3 eV around the maximum of the HMDS ion energy distribution with steps of 0.25 eV and calculated the sum of these spectra. With this energy range, we cover all maxima of the ion energy distributions for ions in the measured mass range, as deduced from preliminary measurements. Ion mass spectra were checked up to 500 amu. As no species were detected above 300 amu, the ion mass spectra in this work were all recorded up to 300 amu. Despite these precautions, mass discrimination in the quadrupole mass analyzer cannot be avoided. Additionally, lighter ions will diffuse radially more quickly than heavier ions in the collisional supersonic expansion behind the orifice, which can lead to additional discrimination. Correction for both phenomena is not straightforward and comparing abundances of ions for the same admixture with each other can only give a hint on the real ratio of their abundances in front of the sampling orifice.

The mass spectra have been measured with the mass step of 0.1 amu and the signal integrated in the ±0.5 amu range around the mass maximum was used in the bar chart to represent signal intensity. Furthermore, the measured ion mass spectra have been normalized to the sum of the counts in the whole spectrum to improve comparability between different admixtures and to correct for changes in the mass spectrometer sensitivity over the course of a measurement series. The sum of measured total counts in each mass spectrum are shown in Figure 3 for argon (×) and helium (◊) in the photon-generating plasma in the studied admixture range. The case with no admixture refers to a mass spectrum taken with no flow through the bubbler. However, residual HMDS desorbing from the tube walls was still visible in the mass spectrum. The absolute measured signal intensities are dependent on the mass-dependent ion transmission function (discriminating heavier ions[62]), on the quality of the mass spectrometer tuning, and on the aging of the secondary electron amplifier detector, so it is not possible to draw reliable conclusions by comparing absolute values as measured with photons from helium or argon plasma. However, the trends measured for each plasma provide valuable information. Impurities dominate the gas mixture at zero HMDS admixture and contribute to the mixture measurably at the lowest HMDS admixtures. As shown in Figure 2, the VUV photons from the helium plasma can photoionize all impurities and that is why the sum of the ion signal is the highest at the zero HMDS admixture. As mentioned above, HMDS is still visible in the spectrum, but the relative abundance at the mass 146 amu is only at around 0.06, while the dominant ion is the one at 73 amu with 0.43 relative abundance. In this case, the signal at this mass is expected to be dominated by the protonated water cluster $(H_2O)_4H^+$. With the argon plasma emission, an increase of the total signal is observed from zero admixture up to 250 ppm first, because the typical impurities cannot be photoionized by argon excimer emission. The relative abundance at the mass 146 amu is, therefore, still at 0.4 even at zero HMDS admixture.

From zero admixture in the case of photons from the helium plasma and 250 ppm for photons from the argon plasma, the total signal decreases strongly with increasing admixture, which influences the relative abundances that will be discussed in the following sections. This is explained mainly by the photons being absorbed higher up in the gas channel when more HMDS is present and fragments need to travel a longer distance to the orifice,

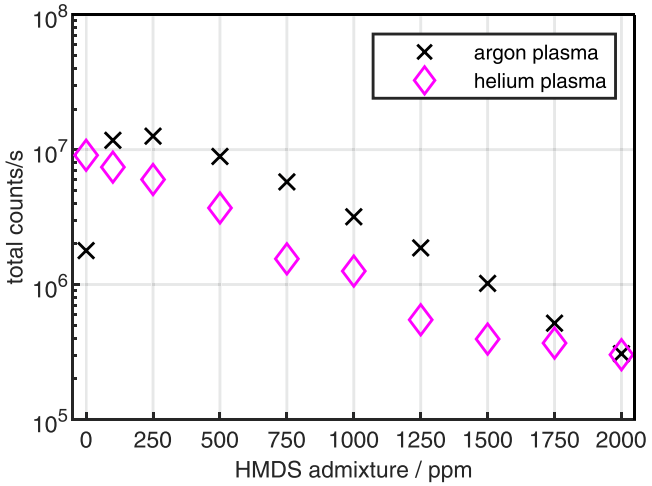

FIGURE 3 The sum of total counts in the measured ion mass range from 10 amu to 300 amu and for 13 ion energies for hexamethyldisilane (HMDS) admixtures from no admixture to 2000 ppm admixed to 800 sccm argon (×) or helium (◇) in the crossing channel of the Capillary-Photon-Jet. The gas flow through the plasma was 400 sccm argon or helium respectively and the generator power was set to 10 W.

which leads to more collisions with subsequent recombination to neutral products or molecular ion polymerisation to heavier ions, which are detected with lower probability. Additionally, more ions are also lost to the horizontal exhaust channel when generated mainly near the channel intersection. Using an absorption cross-section of 1.5×10^{-16} cm^2/molecule at 125 nm,[63] we obtain a penetration depth for photons in HMDS of 27 mm for 100 ppm and 1.4 mm for 2000 ppm admixture, the former one being much longer than the length of the vertical channel, the latter being much shorter (compare Figure 1).

Verification of the assignment of species to measured peaks is performed via calculation of the signal of the species isotopes based on the signal of the parent peak and considering the isotope probabilities of the atoms in the assigned molecular ion.

4 | RESULTS AND DISCUSSION

In the following section, the ionic deposition and photochemistry of HMDS diluted in argon or helium and initiated by photons from an argon or helium plasma respectively, are discussed based on the positive ion mass spectra for HMDS admixtures between 100 and 2000 ppm and on the properties of the deposited thin films. This admixture range covers the conditions with low and high VUV photon absorption. Due to the difference in the emitted photon energy for both gases, we can also compare the effect of ionization of impurities.

4.1 | Overview mass spectra

The positive ion mass spectra in a range between 10 and 300 amu for HMDS-admixtures of 100 ppm (■) and 2000 ppm (■) to argon and helium with argon or helium plasma emission respectively are shown in Figure 4. With the photons generated by the argon plasma, signals of Ar^{2+} (20 amu), Ar^+ (40 amu), and Ar_2^+ (80 amu) have been observed. These ions can only be produced in the discharge and the fact that they are observed indicates, that the gas flow at the channel intersection is not laminar but turbulent and that some gas from the plasma channel can reach the sampling orifice of the mass spectrometer. Assuming the transport time of 2 ms and diffusion constant in the order of 1×10^{-5} m^2 s^{-1}, a diffusion length of 0.14 mm is obtained, smaller than the channel radius. Still, we assume that most of the species coming from the plasma are diverted to the exhaust channel. Even though this section of the mass spectrum is not shown, no helium-related ions (He^+ or He_2^+) have been observed in the case of helium plasma in the capillary, indicating that the flow of helium gas is probably in the laminar regime due to its lower viscosity when compared with argon.

The main feature in the ion mass spectra for both shown admixtures to argon is the peak of the HMDS ion with a mass of 146 amu. It is highlighted in Figure 4 by a black arrow (→) with the associated mass. Based on the isotope abundances calculated from the measured abundance of the parent peak at 146 amu, the peaks from 147 to 150 amu are assigned to the HMDS ions with the variety of isotopes of the constituting atoms. Adding up the relative abundances of HMDS and its two highest isotope peaks, one obtains abundances of 0.92 and 0.75 for 100 ppm and 2000 ppm, respectively. Its dominance is explained by its low ionization energy of 8.27 eV when compared with the feed gas impurities listed in section 2.1. Additionally, the HMDS ion is effectively stabilized by collisions with the background gas. During a study on dissociative photoionization of HMDS, Dávalos and coworkers obtained rate constants in the order of 1×10^{10} s^{-1} for the dissociation of $HMDS^+$ ions after photoionization of neutral HMDS with photon energies above 9.6 eV via breaking of the Si–Si bond or loss of a methyl group.[8] The collision rate in atmospheric pressure plasmas is around 1×10^{11} s^{-1}, meaning that each ion undergoes a number of collisions before potential dissociation, being effectively stabilized even in the case of helium excimer emission discussed later.

These results confirm, that the photons from the argon plasma are almost exclusively ionizing the precursor, thus strongly reducing the influence of impurities on the photochemistry. We will, therefore, focus on the results obtained with argon plasma as the source of the VUV photons.

Still, the comparison to the helium case provides interesting information about the processes in the CPJ. The HMDS ion is the dominant species only at 100 ppm admixture with an abundance of 0.73 and its relative abundance decreases strongly down to 0.04 with increasing admixture, again taking the two highest isotope peaks into account. This decrease can be explained by the decreasing total ion signal (see section 3), while the signals of some impurities are only weakly admixture dependent. Therefore, the relative signals of these impurities will strongly increase, while the relative signals of HMDS-related species decrease. Based on the work of Dávalos and coworkers, the trimethylsilyl ion at 73 amu should be the dominant ion from dissociative photoionization at the high photon energies from the helium plasma.[8] The fact that the

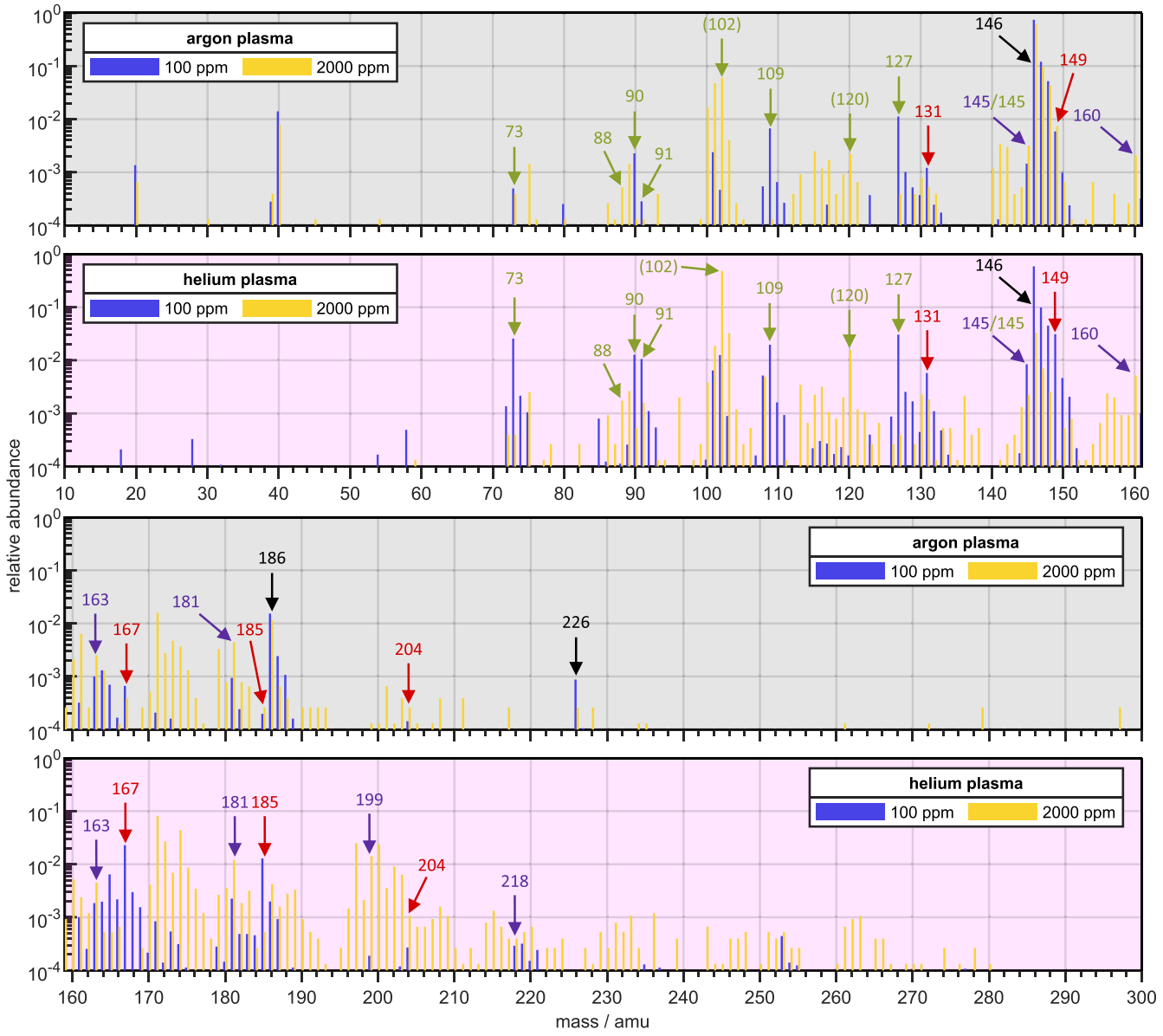

FIGURE 4 Ion mass spectra between 10 and 300 amu for hexamethyldisilane (HMDS) admixtures of 100 (■) and 2000 ppm (■) admixed to 800 sccm argon (upper figures for each mass range) or helium (lower figures for each mass range) in the crossing channel of the Capillary-Photon-Jet. The gas flow through the plasma was 400 sccm argon or helium, respectively. The species associated with HMDS (→) and the three main HMDS-fragments trimethylsilyl (73 amu, →), pentamethyldisilanyl (131 amu, →) and pentamethyldisilylmethyl (145 amu, →) are marked by arrows with the associated masses.

monomer ion is dominant at low admixtures is again attributed to the collisional stabilization as discussed above. However, the relative abundance of trimethylsilyl is higher for the helium plasma emission than for the argon plasma emission very probably due to the higher photon energy. Additionally, the quenching in collisions with helium atoms can have different (slower) rates compared with argon.

The main fragments are produced from HMDS via breaking of the Si–Si, Si–C, and C–H bonds of the molecule and appear in the mass spectra for argon and helium plasma radiation. These fragments are trimethylsilyl, pentamethyldisilanyl, and pentamethyldisilylmethyl at 73, 131, and 145 amu, respectively. We decided to use the naming scheme as used by Shi and coworkers for these species in this work.[13] The species from reactions involving trimethylsilyl are highlighted in Figure 4 by a green arrow (→) and will be discussed in detail in Section 4.3.2 while species from reactions initiated by the pentamethyldisilanyl radical are highlighted by a red arrow (→) and discussed in Section 4.3.3. Species formed in reactions involving pentamethyldisilylmethyl are marked in purple (→) with the discussion of possible reaction pathways in Section 4.3.4. The chemistry is expected to be mainly driven by collisions of these fragments with abundant neutral HMDS. The relative abundance of the three main fragments is higher with the VUV photons from the helium plasma, as more HMDS ions are produced with sufficient excess energy for dissociation. Figure 4 shows an overall higher number of species for the helium plasma radiation, which is explained by the photon energy being above the ionization threshold of feed gas impurities listed in Section 2.1. This is confirmed by the peaks observed at 18, 28, 54 amu at 100 ppm admixture, which are attributed to H_2O^+, N_2^+, and $(H_2O)_3^+$ respectively, and are completely absent with argon plasma photons. The interaction of excited impurities from the plasma effluent with the HMDS could potentially also influence the observed chemistry but we expect this effect to be negligible because we detect argon-related ions coming from the plasma, but no impurity ions such as H_2O^+, N_2^+ or O_2^+. Attachment of abundant water molecules or argon atoms to ions can take place both in the gas phase in the channels at atmospheric pressure or in the supersonic expansion behind the sampling orifice into the mass spectrometer due to adiabatic cooling of the gas. Ions with attached water or argon are ultimately detected as one species with the respective ion mass increased by 18 or 40 amu. In the case of the helium carrier gas, the neutral helium atoms diffuse faster outwards in the expansion, due to their lower weight, so an attachment is less likely. This is confirmed by no visible groups of ions, that share the same trend and are separated by 4 amu.

Unfortunately, not all peaks can be clearly assigned to an impurity or the reaction of an impurity species with a product from HMDS photochemistry. This is especially the case for the ions at 100–102 amu, 171, and 200 amu as we will discuss in Section 4.3.5.

4.2 | Thin-film deposition

As described in Section 2.4, films from HMDS were deposited on silicon wafers and studied in transmission using FTIR spectroscopy. The baseline-corrected and normalized spectra for admixtures of 100, 500, 1000, and 2000 ppm HMDS to argon for a generator power of 25 W are shown in Figure 5. These admixtures cover the range from large to small ratio of impurities to HMDS molecules and also allow us to study the influence of the radiation penetration depth on the deposited films. We chose the higher power compared with the mass spectrometry measurements to deposit more material for a better signal-to-noise ratio in the FTIR spectra. Argon with lower purity (99.999%) was used for the deposition, as it is more cost-efficient and impurities are not expected to mainly originate from the gas bottle but from the gas tubes.

The features identified in the FTIR spectra are listed in Table 1. We observe a strong oxidation of the deposited films, especially at 100 and 500 ppm admixture, where the Si–O–Si peak around 1050 cm^{-1} is by far the highest in the spectrum accompanied only by a very weak signal of or Si–CH_2 at 800 cm^{-1} and Si–CH_3 at 1260 cm^{-1}. This oxidation probably takes place during the deposition, because the impurity/HMDS ratio is highest under these conditions and the Si–O–Si peak is an additional hint corroborating the formation of siloxane species in the gas phase as discussed in Section 4.3.2.[17] Additionally, the VUV photons are not fully absorbed in the gas phase and can reach the substrate in this case, which is probably further enhancing the film oxidation during growth. The maximum of the Si–O–Si peak shifts toward higher wavenumbers with decreasing admixture, coming closer to the typical value of 1075 cm^{-1} of the thermal oxide,[46] which is another indicator for increasing oxygen content of the deposited film.[20]

Interaction of the VUV-radiation with the deposited film must lead to additional carbon removal during deposition, next to the film interacting with oxygen-containing impurities, especially at lower admixtures of 100 and 500 ppm. Carbon removal is otherwise achieved

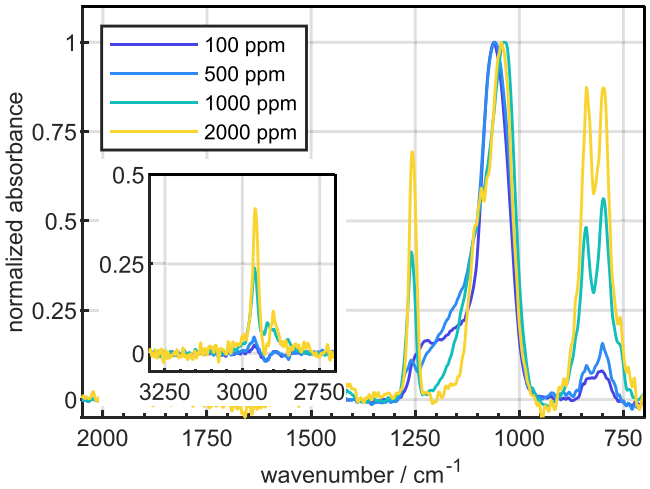

FIGURE 5 Normalized absorbance in a wavenumber range from 2050 to 700 cm^{-1} (inset 3300–2700 cm^{-1}) of thin films deposited from hexamethyldisilane (HMDS) with photons from the argon plasma at 100, 500, 1000, and 2000 ppm admixture to the crossing gas flow of 800 sccm argon. The gas flow through the plasma was 400 sccm argon and the generator power was 25 W.

TABLE 1 Bonds assigned to the features in the FTIR spectra of the films deposited from HMDS with photons from argon plasma in Figure 5 with the associated references.

ν/cm^{-1}	Assignment	Literature
2963–2961	ν^a(C-H) in CH_3	2960,[17] 2951,[19] 3000-2860[3]
2907–2897	ν^s(C-H) in CH_3	2893,[19] 3000-2860[3]
1415–1404	ν^a(Si–CH_3), δ(CH_2) in Si(CH_2)$_n$	1405,[17] 1408[19]
1261–1258	δ^s(CH_3) in $SiMe_n$	1260,[3,17] 1246[19]
1059–1034	Si-O-Si, Si-O-C, κ(CH_2) in Si$-(CH_2)_n-Si$	1050,[3,17] 1044,[19] 1000-1030[41]
841–843	CH, δ^s(CH_3) in $SiMe_n$	840,[17] 835[19]
800–798	Si–CH_3, Si–CH_2, Si-C	800,[3,17] 830-800[41]
690	ν(Si-C)	690[19]

Note: The given wavenumbers are the position of the maximum absorption of the feature rounded to full wavenumbers.

by an increase in substrate temperature, which is not a viable option for sensitive substrates.[41] The interaction of the VUV-radiation with the substrate has been studied before for polymer surfaces with the conclusion that mainly trimethylsilyl radicals react with free surface sites created by the radiation.[50] Other authors suggest a different scheme for film formation from HMDS in plasma-enhanced chemical vapor deposition experiments based on highly reactive transient species from the gas phase like 1,1-dimethylsilene (see Section 4.3.2) performing polymerization reactions at the surface.[10,41] Active sites for the insertion of gas-phase radicals and impurities may in our case also be created in the forming film by the VUV-radiation. The observation of Si–CH_2 bonds in the IR spectra supports the assumption that this film growth mechanism at least partly contributes to film formation in our experiments. At the high end of the studied admixture range, the ratio of supplied HMDS to oxygen-containing impurities increases, while photons are effectively absorbed by the precursor before they can interact with the substrate. Deposition is in this case mainly based on $HMDS^+$, leading to an increase of CH_x bonds and probably Si-CH_2-Si bonds. The relatively narrow peaks indicate that the films are weakly cross-linked and polymer-like, as expected for deposition at atmospheric pressure.[41]

The Si–Si bonds cannot be measured with infrared absorption. However, atomic oxygen readily inserts into Si–Si bonds, converting them to Si–O–Si.[64] The FTIR-spectra also show that little oxygen is bound to carbon, probably due to a small number of carbon active sites, as they are mostly populated by hydrogen. The absence of Si–H bonds around 2200 cm^{-1} suggests either a small contribution of species with these bonds like trimethylsilane ions ($TriMS^+$) or the $HMDS^+$ isomer to the film formation or a loss of these weaker bonds after deposition. This may be again caused by the interaction of the VUV radiation with the surface, removing the hydrogen atoms and thus creating active sites at silicon for the addition of oxygen or other radicals.[20] The interaction of species participating in film formation with active sites at silicon is further enhanced by the fact that in deposited ions, a silicon atom will mostly carry the positive charge, due to its lower electronegativity when compared to carbon or hydrogen. Especially the formation of bonds between silicon or carbon and oxygen is energetically favorable, as they are stronger than Si–Si or Si–C bonds.[19]

Film properties could be modified by increasing the substrate temperature or by substrate biasing, which will increase the incident ion energy. Bringing the photochemistry closer to the surface will additionally increase the yield of reactive species transported onto the substrate. Moving to attenuated total reflection FTIR (ATR-FTIR) opens the possibility for deposition on noninfrared-transparent substrates like polymers. The modification of polymer surfaces by VUV-radiation with simultaneous deposition from organosilicon precursors has shown to produce films with good adhesion and unique properties.[50,65]

4.3 | VUV photochemistry of HMDS

We observed a large number of ions produced by photoionization of HMDS and subsequent reactions in the mass spectra. Table 2 shows the identified species from HMDS photochemistry with their mass and chemical composition. A detailed analysis of the species associated with these ions and possible formation pathways are discussed in this section as far as a clear assignment of species to the measured peaks is possible. In the discussion of the photochemistry, one needs to keep in mind, that only a small number of HMDS molecules are ionized by the radiation due to the photon flux from the plasma. A rate of 4.8×10^{11} molecules/s contributing to film growth at the substrate can be estimated with a measured film thickness of around 30 nm and assuming for simplicity a disk-shaped deposit with a diameter of 2 mm, a density of 1.1 g cm^{-3}[47] and that only HMDS ions are deposited. This means, that the photon flow emitted by the plasma in the direction of the precursor must be in the same order of magnitude, which is significantly below the flow of HMDS molecules into the source. This number can be estimated via the volume flow of 800 sccm and the number density 2.45×10^{21} m^{-3} of HMDS at the lowest admixture of 100 ppm to be around 3.3×10^{16} molecules/s. This estimation leads to

TABLE 2 HMDS fragment ions and polymerization products identified in the positive ion mass spectra for helium and argon plasma generated photons in Figure 4.

Mass/amu	Linear formula	Composition	Formation
58	$Me_2Si^{\bullet\bullet+}$	C_2H_6Si	M-88
72	$Me_2Si = CH_2^+$	C_3H_8Si	M-74
73	**$Me_3Si^{\bullet+}$**	**C_3H_9Si**	**M-73**
74	Me_3SiH^+	$C_3H_{10}Si$	M-74, 73+1
88	Me_4Si^+	$C_4H_{12}Si$	73+15, M-58
90	Me_3SiOH^+	$C_3H_{10}SiO$	72+18, 73+17
91	$Me_3Si^{\bullet+} \cdot H_2O$	$C_3H_{11}SiO$	73+18
(102)	$Me_3SiCH_2CH_3^+$	$C_5H_{14}Si$	73+29
109	$Me_3Si^{\bullet+} \cdot (H_2O)_2$	$C_3H_{13}SiO_2$	73+2x18
(120)	$Me_3SiCH_2CH_3^+ \cdot H_2O$	$C_5H_{14}Si$	102+18
127	$Me_3Si^{\bullet+} \cdot (H_2O)_3$	$C_9H_{15}SiO_3$	73+3x18
131	**$Me_3SiSiMe_2^{\bullet+}$**	**$C_5H_{15}Si_2$**	**M-15**
132	$Me_3SiSiMe_2H^+$	$C_5H_{16}Si_2$	131+1
145	**$Me_3SiSiMe_2CH_2^{\bullet+}$**	**$C_6H_{17}Si_2$**	**M-1**
146	**$Me_3SiSiMe_3^+$** ($Me_3SiCH_2SiMe_2H^+$)	**$C_6H_{18}Si_2$**	**M**, isomer
149	$Me_3SiSiMe_2^{\bullet+} \cdot H_2O$	$C_5H_{17}Si_2O$	131+18
160	$Me_3SiSiMe_2CH_2CH_3^+$	$C_7H_{20}Si_2$	145+15
163	$Me_3SiSiMe_2CH_2^{\bullet+} \cdot H_2O$	$C_6H_{19}Si_2O$	145+18
167	$Me_3SiSiMe_2^{\bullet+} \cdot (H_2O)_2$	$C_5H_{19}Si_2O_2$	131+2x18
181	$Me_3SiSiMe_2CH_2^{\bullet+} \cdot (H_2O)_2$	$C_6H_{21}Si_2O_2$	145+2x18
185	$Me_3SiSiMe_2^{\bullet+} \cdot (H_2O)_3$	$C_5H_{21}Si_2O_3$	131+3x18
186	$Me_3SiSiMe_3^+ \cdot Ar$	$C_6H_{18}Si_2Ar$	M+40
199	$Me_3SiSiMe_2CH_2^{\bullet+} \cdot (H_2O)_3$	$C_6H_{23}Si_2O_3$	145+3x18
204	$Me_3SiSiMe_2SiMe_3^+$	$C_8H_{24}Si_3$	131+73, M+58
218	$Me_3SiSiMe_2CH_2SiMe_3^+$	$C_9H_{26}Si_3$	145+73
226	$Me_3SiSiMe_3^+ \cdot 2Ar$	$C_6H_{18}Si_2Ar_2$	M+2x40

Note: The monomer ion and the three main fragment ions are highlighted.

the conclusion, that fragments produced in photolysis of the monomer are mainly colliding with the argon background, neutral HMDS molecules, and impurities with abundances in the order of a few ppm with decreasing probability. Reactions between fragments are therefore very improbable and the chemistry is dominated by species directly produced from HMDS or in secondary reactions with HMDS or impurities.

Additionally, table 2 shows the species associated with water impurities. Great sensitivity of HMDS chemistry to traces of water and oxygen has been reported before, so further purification and handling of the liquid HMDS under dry nitrogen or argon atmosphere as well as storage under vacuum is advised.[10,18,19,50,66,67] Due to limitations of the setup and the storage, HMDS was transferred as delivered to the bubbler under ambient conditions and the bottle was stored in a normal chemical cabinet. We expect, therefore, impurities from the precursor to influence the observed photochemistry.

4.3.1 | $HMDS^+$ ions

The $HMDS^+$ ion with a mass of 146 amu is formed by photoionization of the HMDS molecule

$$Me_3SiSiMe_3 \xrightarrow{h\nu} Me_3SiSiMe_3^+ + e^-. \quad (1)$$

Figure 6 shows the relative abundance of the $HMDS^+$ ion and species formed by argon attachment leading to ions with 186 and 226 amu. This assignment is confirmed by the isotope signals of these species and the slowly decreasing trend of the relative abundance with increasing admixture. We chose to only show the abundances with the argon plasma photons here, due to the expected reduced influence of impurities on the photochemistry. Interestingly, water attachment to the HMDS ion seems to be less effective than attachment to species with an unpaired electron like pentamethyldisilylmethyl at 145 amu. The ratio between the abundances measured at 163 and 164 amu as well as 181 and 182 amu (from attachment of one or two water molecules, respectively) is a lot higher than the ratio between the abundances at 145 and 146 amu.

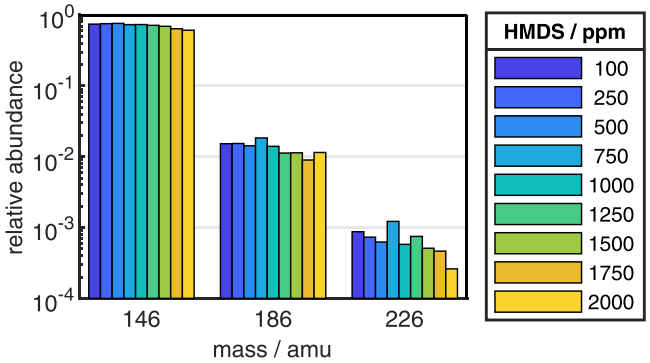

FIGURE 6 Relative abundance of hexamethyldisilane (HMDS) and species associated with argon attachment to HMDS ions as a function of HMDS admixture in a range from 100 to 2000 ppm admixed to 800 sccm argon in the crossing channel of the Capillary-Photon-Jet. The gas flow through the plasma was 400 sccm argon and the generator power was set to 10 W.

During basic studies of HMDS-pyrolysis, isomerization of HMDS to dimethyl(trimethylsilylmethyl)silane ($Me_3SiCH_2SiMe_2H$) has been observed at different temperatures and pressures[68–74] and explained via a chain process involving radical rearrangement at elevated pressures. The formation of the isomer has also been observed in mercury-photosensitized decomposition of HMDS[74] and in low-pressure photolysis at 206 nm,[75] but via a different reaction pathway in the latter case. Formation of the isomer may take place in our case as well, possibly via collisionally stabilized radicals. The isomer influences the chemistry due to the weaker Si–H bond when compared with the C–H bond of HMDS. We will discuss a possible participation of the isomer and its fragments in reactions later in the text.

4.3.2 | Trimethylsilyl$^+$ ions

Dissociative photoionization is expected to be the source of the ions at 73 amu via

$$Me_3SiSiMe_3 \xrightarrow{h\nu} Me_3Si^{\bullet +} + Me_3Si^{\bullet} + e^-, \quad (2)$$

leading to two trimethylsilyl radical fragments, one of which is ionized. The species from reactions involving trimethylsilyl are highlighted in Figure 4 by a green arrow (→) and text and their relative abundance as a function of HMDS admixture irradiated by the argon plasma is shown in Figure 7 in the studied admixture range. The trimethylsilyl ion has a low relative abundance in the order of 5×10^{-4} with the argon plasma photons, which is approximately constant. Its abundance is much higher when interacting with the helium plasma emission with 0.03 for 100 ppm admixture and shows a strong decrease with increasing admixture again down to around 5×10^{-4}. The overall low abundance is explained, in addition to the collisional stabilization of the monomer ion, by trimethylsilyl being involved in polymerization reactions. More trimethylsilyl is

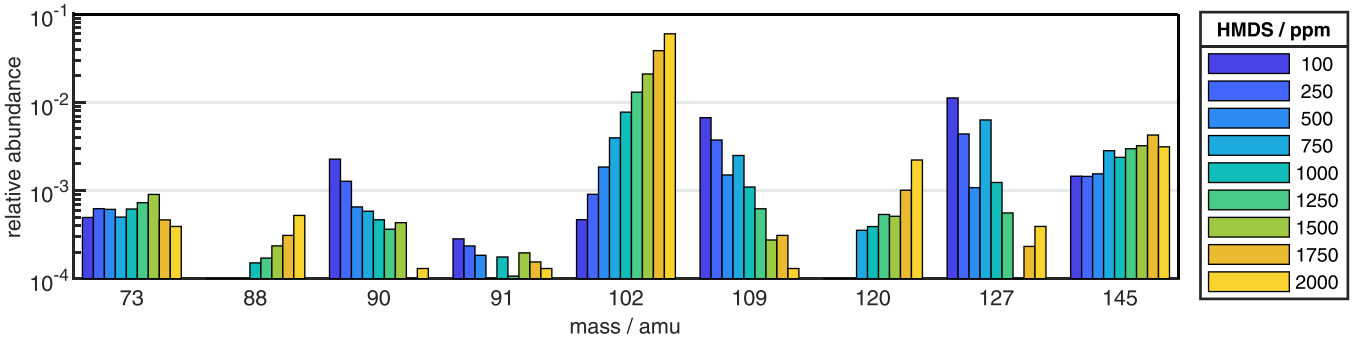

FIGURE 7 Relative abundance of species associated with reactions involving trimethylsilyl as a function of hexamethyldisilane (HMDS) admixture in a range from 100 to 2000 ppm admixed to 800 sccm argon in the crossing channel of the Capillary-Photon-Jet. The gas flow through the plasma was 400 sccm argon and the generator power was set to 10 W.

produced by the photons of the helium plasma as they possess a higher energy leading to a higher probability for dissociative ionization. For the argon plasma radiation, the relative abundance of the trimethylsilyl ion approximately resembles the abundance trend of the HMDS ion. This suggests, that the formation of trimethylsilyl is directly coupled to the formation of $HMDS^+$.

Fragmentation of the Si–Si bond has been reported to be the main decomposition channel in pyrolysis[68,70,71,74] and photolysis.[48,49,75] Several authors studied the decomposition of HMDS on a hot filament under low-pressure conditions using VUV ionization mass spectrometry at 118 nm and obtained reference mass spectra at room temperature that can be compared with the mass spectra obtained in this work due to the photon energy in the same range.[13,76] In these works, the trimethylsilyl ion was the main photofragment of HMDS as well. An additional source of trimethylsilyl may be fragmentation of HMDS by excited hydrogen atoms from the plasma effluent or from hydrogen loss from HMDS during ionization, the second product being TriMS with 74 amu.[32,59]

Due to the reasons named above, the peak at 73 amu is not assigned to the protonated water cluster $(H_2O)_4H^+$ for the low-energy photons from the argon plasma. With helium plasma photons, it is still likely that only a small fraction of the ion detected at 73 amu is from the respective water cluster because the water cluster ion has a much higher ionization energy when compared with HMDS and the trimethylsilyl fragment (7.03 eV[67]). The onset energy for dissociative photoionization of HMDS is 9.662 eV for production of trimethylsilyl which is around the mean energy of argon excimer emission energy range, so mainly production of this fragment in our source is expected. The Si–Si bond dissociation energy is 3.45 eV, which makes it the weakest bond in the HMDS molecule.[8]

1,1-dimethylsilene and TriMS with masses of 72 and 74 amu can be produced directly via dissociative ionization of HMDS in reaction[13,48,49,75]

$$Me_3SiSiMe_3 \xrightarrow{h\nu} \begin{cases} Me_3SiH^+ + Me_2SiCH_2 + e^-, \\ Me_3SiH + Me_2SiCH_2^+ + e^-, \end{cases} \quad (3)$$

by an intramolecular hydrogen transfer reaction.[74] 1, 1-dimethylsilene has a high reactivity leading to the overall low abundance of this species.[77]

TriMS is additionally formed via hydrogen abstraction from HMDS by trimethylsilyl[13,48]

$$Me_3Si^{\bullet +} + Me_3SiSiMe_3 \longrightarrow Me_3SiH^+ + Me_3SiSiMe_2CH_2^{\bullet}, \quad (4)$$

leading to the pentamethyldisilylmethyl radical with 145 amu. Due to the weaker Si–H bond compared with the C–H bond broken, hydrogen abstraction is endothermic[66] and proceeds therefore in our case only when trimethylsilyl ions or neutrals have excess energy from reaction 2, which explains the lower abundance of TriMS with the argon plasma emission. A clear separation from the isotopes of the trimethylsilyl ion was not possible for both types of plasma radiation, as the Si–H bond makes it prone to hydrogen abstraction or insertion reactions.[73,74] Charge transfer from a trimethylsilyl ion to neutral HMDS during reaction 4 is not expected due to the lower ionization potential of trimethylsilyl when compared with the monomer, so the TriMS will keep the charge. In a reaction between neutral trimethylsilyl from reaction 2 and an HMDS ion, charge transfer could happen and would again lead to the formation of a neutral pentamethyldisilylmethyl radical. Additionally, the ionization potential of TriMS is higher than the one of HMDS, so charge transfer to abundant neutral HMDS is another possible loss channel for TriMS ions[78]

$$Me_3SiH^+ + Me_3SiSiMe_3 \longrightarrow Me_3SiH + Me_3SiSiMe_3^+. \quad (5)$$

Hydrogen abstraction has a lower energy barrier for the Si–H bond of the HMDS isomer, contributing to the peak at 145 amu with a rearranged version of pentamethylsilylmethyl.[66] The chemistry involving this radical will be discussed in Section 4.3.4.

In addition to hydrogen abstraction, methyl abstraction from HMDS by a trimethylsilyl radical also takes place

$$Me_3Si^{\bullet+} + Me_3SiSiMe_3 \longrightarrow Me_4Si^+ + Me_3SiSiMe_2, \quad (6)$$

forming mainly neutral pentamethyldisilanyl (131 amu) and ionized tetramethylsilane (TMS, 88 amu) in the process.[13] TMS ions are mainly observed at high admixtures for both plasma gases, which could be partially explained by the higher ionization threshold of TMS when compared with HMDS leading to TMS loss in charge transfer reactions with abundant HMDS.[78] The increasing relative abundance of TMS, while the trimethylsilyl abundance stays approximately constant (see Figure 7), indicates that another reaction must contribute to TMS production. An alternative pathway for the formation of TMS, reported in high-pressure pyrolysis and photolysis, is via direct decomposition of HMDS with intramolecular elimination of a methyl group

$$Me_3SiSiMe_3 \xrightarrow{h\nu} \begin{cases} Me_4Si^+ + Me_2Si^{\bullet\bullet} + e^-, \\ Me_4Si + Me_2Si^{\bullet\bullet+} + e^-, \end{cases} \quad (7)$$

the second possibly ionized fragment being dimethylsilylene (58 amu).[13,49,73–75] We measured a very low signal of dimethylsilylene ions with 100 ppm HMDS in helium, indicating that its production is increased by the higher energy photons from the helium plasma, probably due to the fact, that reaction 7 requires more energy than normal HMDS dissociation. This and the high reactivity of this radical ion with two unpaired electrons explains its low abundance and the absence in the mass spectra for the argon case. The references above also state, that the insertion of dimethylsilylene into a C–H bond of HMDS takes place and forms a molecule with 204 amu:

$$Me_2Si^{\bullet\bullet+} + Me_3SiSiMe_3 \longrightarrow Me_3SiSiMeCH_2SiMe_2H^+. \quad (8)$$

This species possesses a Si–H bond prone to abstraction or photofragmentation, leading to a radical with 203 amu. Dimethylsilylene readily inserts into existing Si–H bonds[75,79] of, for example, the HMDS isomer forming a molecule with again 204 amu.

The large signal and the relative trend with admixture measured at 102 amu are unexpected and difficult to explain. It could be partly from ethyltrimethylsilane ions, which are formed in a reaction between the TMS fragment with 87 amu and a methyl radical with 15 amu.[13,80] However, based on the isotope probabilities of ethyltrimethylsilane, another ion with the same mass must contribute to the signal. This is why we discuss the influence of the plasma itself in Section 4.3.5. Hydrogen loss from ethyltrimethylsilane could lead to the formation of the species detected at 101 amu, while the species at 100 amu may be from the reaction of a vinyl radical (C_2H_3) with trimethylsilyl. As the isotope signals of the latter two species are overlapping with the signals of the species at 101 and 102 amu, no definite statement on the origin of the measured signals can be made.

Water attachment to trimethylsilyl has been observed before and produces the ions detected at 91, 109, 127 amu, and partly 145 amu in our case.[81] The relative abundances of the first three ions decrease with increasing admixture due to the simultaneous decrease of water impurity densities relative to the HMDS density. This can be again explained by the position at which the ions are produced in the vertical gas channel. The signal at 145 amu overlaps with the signal of pentamethyldisilylmethyl and therefore shows a slow increase in relative abundance, which indicates that this HMDS fragment is produced more effectively with increasing number of HMDS molecules. This behavior will be discussed in Section 4.3.4.

The signals at 89 and 90 amu are assigned in the literature to trimethylsilamine ($Me_3SiNH_2^+$) and trimethylsilanol (Me_3SiOH^+) from the reaction of 1,1-dimethylsilene with ammonia or water.[49,75,77,82] The ion detected at 75 amu may be a fragment of trimethylsilanol having lost a methyl group, while hydrogen loss from trimethylsilanol is also expected to contribute to the measured signal at 89 amu. However, in a pyrolysis study of HMDS diluted in N_2, an increase of sample pressure did not change the product yields during irradiation at 147 nm, hinting toward a low influence of nitrogen on photochemistry at this wavelength.[83] This means that if atomic nitrogen contributes to the formation of observed ionic species, it must be from the plasma, which is very improbable, as explained above. The contribution of 1,1-dimethylsilene to the production of the ions at 75 and 89 amu however, is indicated by the similar dependence of their relative abundance on admixture. Subsequent reactions may produce hexamethyldisilazane ($Me_3SiNHSiMe_3$, 161 amu, same relative trend as 75 and 89 amu) and HMDSO (162 amu), contributing to the

signals at these masses. The weaker signal at 162 amu, which is additionally overlapped by the isotope signal of the ion at 161 amu, is connected with the small photolysis cross-section of HMDSO when compared with other organosilicon precursors.[84] This is also the reason for the small contribution of the HMDSO impurity in HMDS to the observed chemistry (see Section 2.2). However, direct interaction of atomic oxygen with the precursor also forms species with masses observed in our spectra especially by insertion into the Si–Si bond.[64] Unfortunately, there is no information on the photolysis cross-section of these species, so their contribution to the measured signals can not be estimated.

4.3.3 | Pentamethyldisilanyl$^+$ ion

The signal at 131 amu confirms that breaking of the Si–C bond in HMDS also occurs during dissociative photoionization and leads to the formation of a pentamethyldisilanyl ion and a free methyl radical via[49]

$$Me_3SiSiMe_3 \xrightarrow{h\nu} Me_3SiSiMe_2^{\bullet +} + CH_3^{\bullet} + e^-. \quad (9)$$

Due to the lower electronegativity of silicon when compared with carbon, the positive charge will most likely be on a silicon atom in the pentamethyldisilanyl radical. The complete absence of CH_3^+ in the mass spectra supports this assumption. Another explanation for that is the ionization potential of CH_3, which is above the threshold for HMDS with 9.84 eV,[85] enabling charge transfer reactions from CH_3^+ to abundant neutral HMDS. The bond dissociation energy of the Si–C bond has been determined to be 3.63 eV, so slightly above the dissociation energy of the Si–Si bond, leading to a lower abundance of pentamethyldisilanyl in the order of 1×10^{-3} and decreasing with admixture.[74] Species associated with this radical are marked with a red arrow () and text in Figure 4 and their relative abundance with photons from the argon plasma as a function of HMDS admixture is shown in Figure 8. As with trimethylsilyl, the relative abundance of the pentamethyldisilanyl ion follows the trend of the HMDS ion, which indicates, that the production of HMDS $^+$ and pentamethyldisilanyl are connected and the main formation channel of this species is via reaction 9.

As neutral HMDS molecules are again the main collision partner for pentamethyldisilanyl ions, the three main reactions involving this ion are hydrogen, methyl, and possibly trimethylsilyl abstraction from HMDS. While methyl abstraction reforms starting material, endothermic hydrogen abstraction forms pentamethyldisilane ions (PMDS $^+$) with 132 amu and a neutral pentamethyldisilylmethyl radical:

$$Me_3SiSiMe_2^{\bullet +} + Me_3SiSiMe_3 \longrightarrow Me_3SiSiMe_2CH_2^{\bullet} + Me_3SiSiMe_2H^+. \quad (10)$$

To our knowledge, there is no literature on the ionization energy of pentamethyldisilanyl, but as with trimethylsilyl, we expect it to be lower than the ionization potential of HMDS. The positive charge will therefore stay on the PMDS molecule. As with TriMS at 74 amu, the signal at 132 amu is approximately as high as the calculated abundance of the isotope signals of pentamethyldisilanyl (131 amu, see Figure 4), so PMDS may be lost in charge transfer reactions with neutral HMDS molecules. The ionization threshold of PMDS should be below 10.2 amu,[78] however, no specific value is given in the literature.

Formation of an octamethyltrisilane ion with 204 amu may be possible via abstraction of a trimethylsilyl radical from HMDS,

$$Me_3SiSiMe_2^{\bullet +} + Me_3SiSiMe_3 \longrightarrow Me_3Si^{\bullet} + Me_3SiSiMe_2SiMe_3^+, \quad (11)$$

forming neutral trimethylsilyl in the process. Detailed information on the bond energies in octamethyltrisilane is unfortunately not available, so we can only assume, that the bond dissociation energy of the Si–Si bond in HMDS is approximately the same as the bond energy between the silicon atoms in octamethyltrisilane, so this abstraction reaction has no energy barrier. The relative abundance of this species increases with admixture, possibly indicating an increase in polymerization reactions, however, its relative abundance is very low. The chemistry of octamethyltrisilane

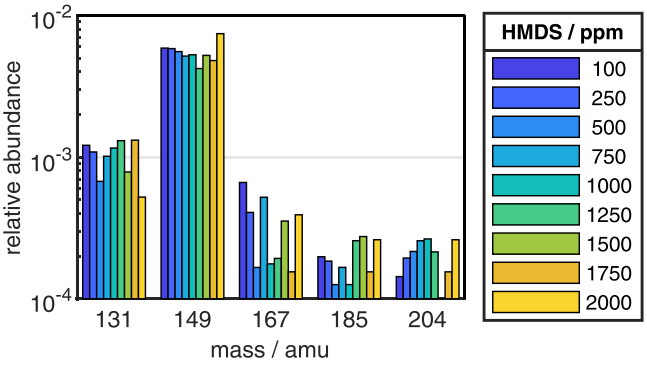

FIGURE 8 Relative abundance of species associated with reactions involving pentamethyldisilanyl as a function of hexamethyldisilane (HMDS) admixture in a range from 100 to 2000 ppm admixed to 800 sccm argon in the crossing channel of the Capillary-Photon-Jet. The gas flow through the plasma was 400 sccm argon and the generator power was set to 10 W.

is a complex topic on its own, as decomposition and isomerization can take place after formation.[86]

The contribution of neutral methyl radicals formed in reaction 9 to the overall chemistry can not be easily assessed. Subsequent photoionization of these radicals is very improbable due to the low photon flux compared with the number of neutral HMDS molecules supplied to the source, even though the photon-energy from the argon plasma would be sufficient to ionize methyl. Hydrogen or methyl abstraction from neutral HMDS may be a quick follow-up reaction, however, the products methane (CH_4) and ethane (C_2H_6) are absent from our spectra even with the higher-energy radiation from the helium plasma. This is mainly attributed to the low ionization probability due to the reason stated above and their high ionization energies, meaning that produced ions are quickly lost in charge transfer reactions with HMDS.

In addition to the signal of the isotopes of the HMDS parent ion, a water molecule attached to pentamethyldisilanyl contributes to the measured signal at 149 amu, while the trend is mainly prescribed by the HMDS isotopes. Attachment of water clusters with two and three molecules gives the ions detected at 167 and 185 amu respectively. In contrast to the trend of the species associated with water attachment to trimethylsilyl, the abundances of the species at 167 amu decreases with admixture, which could be connected with the decreasing density of water impurities relative to HMDS, as discussed in Section 4.3.2 for trimethylsilyl. On the other hand, the abundance of the species at 185 amu slightly increases due to the contribution of pentamethyldisilylmethyl ions with an attached argon atom to the signal at this mass.

4.3.4 | Pentamethyldisilylmethyl$^+$ ion

In addition to reactions 4 and 10, pentamethyldisilylmethyl can be produced by the loss of one hydrogen atom from HMDS during photoionization

$$Me_3SiSiMe_3 \xrightarrow{h\nu} Me_3SiSiMe_2CH_2^{\bullet +} + H^{\bullet} + e^- . \quad (12)$$

Again, the positive charge is expected to stay on a silicon atom after dissociation. It appears in our measurements with an abundance in the range of 1×10^{-3} to almost 1×10^{-2} for the low admixture and the helium plasma emission case. The higher abundance with helium and the decrease with admixture is again explained by the reasons stated above for the trimethylsilyl and pentamethyldisilanyl radicals. The C–H bond is the strongest bond in the HMDS molecule with around 4.15 eV. The chemistry involving pentamethyldisilylmethyl is highlighted in Figure 4 in purple (→) and the abundance of the associated species with argon plasma radiation is shown in Figure 9 as a function of admixture. The relative abundance at 145 amu increases by about a factor of two with increasing admixture. In contrast to trimethylsilyl and pentamethyldisilanyl, its abundance does not follow the abundance of the HMDS ion, indicating additional formation pathways like hydrogen abstraction from HMDS by radicals in reactions 4 and 10, but also by hydrogen atoms and neutral methyl radicals, which were not captured in our measurements.

Methyl abstraction from neutral HMDS by pentamethyldisilylmethyl ions is exothermic, as a Si–C bond is broken and a stronger C–C bond is formed. It leads to the formation of ethylpentamethyldisilane ions with 160 amu and neutral pentamethyldisilanyl

$$Me_3SiSiMe_2CH_2^{\bullet +} + Me_3SiSiMe_3 \longrightarrow Me_3SiSiMe_2CH_2Me^+ + Me_3SiSiMe_2^{\bullet} . \quad (13)$$

The relative abundance of this species shows an even stronger increase with admixture than the pentamethyldisilylmethyl ion, indicating an additional formation pathway or a contribution from impurities, that could not be identified based on the available data.

Formation of 2,2,3,3,5,5-hexamethyl-2,3,5-trisilahexane with 218 amu has been reported in the literature by a reaction between pentamethyldisilylmethyl and trimethylsilyl.[13,75] In our case with the high density of neutral HMDS, it may be formed by exothermic abstraction of a trimethylsilyl radical from HMDS in reaction

$$Me_3SiSiMe_2CH_2^{\bullet +} + Me_3SiSiMe_3 \longrightarrow Me_3SiSiMe_2CH_2SiMe^+ + Me_3Si^{\bullet} . \quad (14)$$

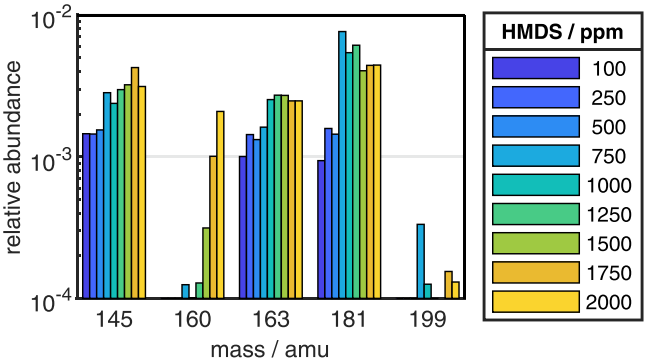

FIGURE 9 Relative abundance of species associated with reactions involving pentamethyldisilylmethyl as a function of hexamethyldisilane (HMDS) admixture in a range from 100 to 2000 ppm admixed to 800 sccm argon in the crossing channel of the Capillary-Photon-Jet. The gas flow through the plasma was 400 sccm argon and the generator power was set to 10 W.

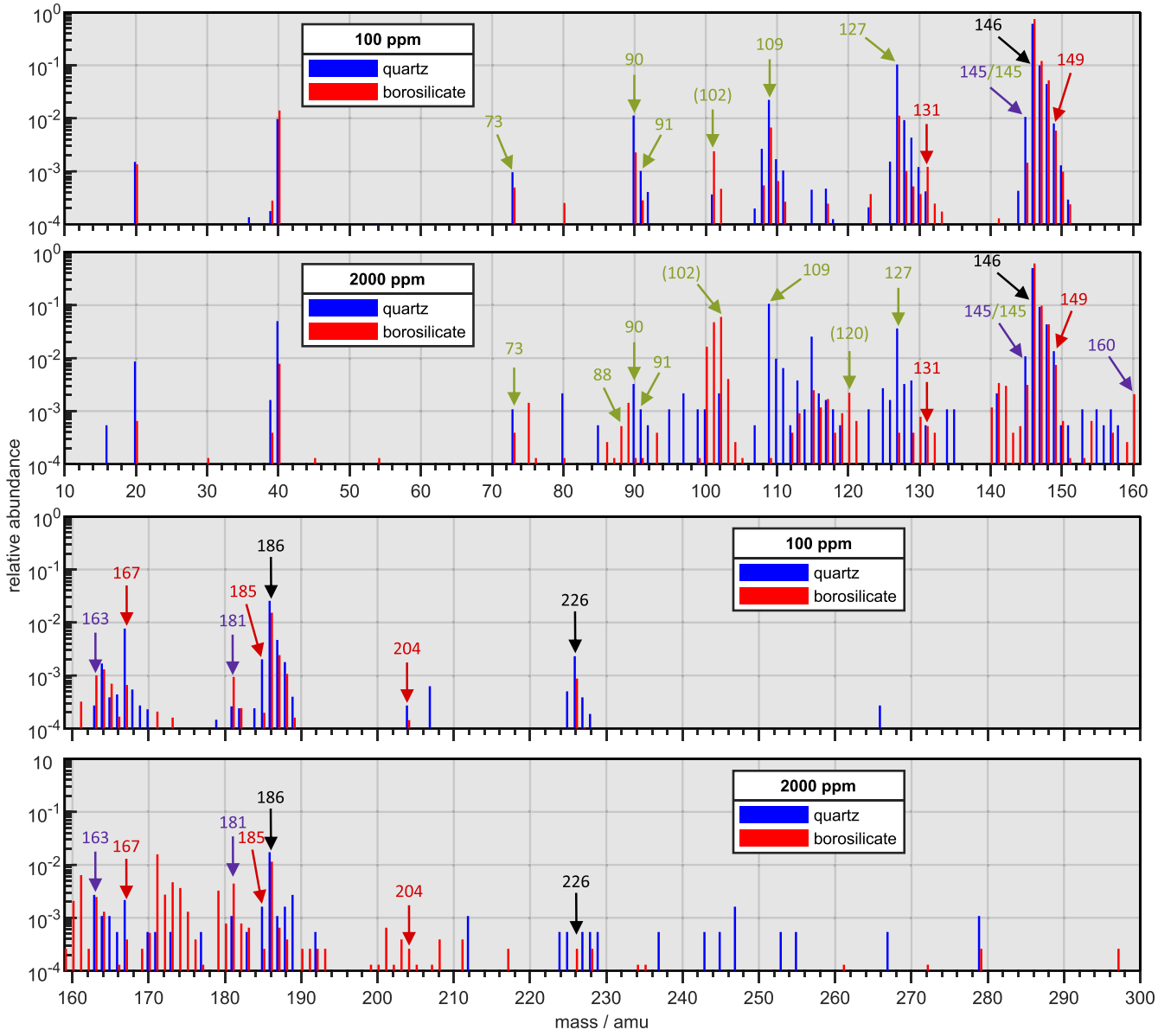

FIGURE 10 Ion mass spectra between 10 and 300 amu measured with quartz (■) and borosilicate (■) capillary as dielectric in front of the electrodes for hexamethyldisilane (HMDS) admixtures of 100 (upper figures for each mass range) and 2000 ppm (lower figures for each mass range) admixed to 800 sccm argon in the crossing channel of the Capillary-Photon-Jet. The gas flow through the plasma was 400 sccm argon. The species associated with HMDS (→) and the three main HMDS-fragments trimethylsilyl (73 amu, →), pentamethyldisilanyl (131 amu, →), and pentamethyldisilylmethyl (145 amu, →) are marked by arrows with the associated masses.

A rearranged version of this molecule can be formed with the rearranged pentamethyldisilylmethyl from the HMDS isomerization.[49] This ion is only visible at 2000 ppm with the argon plasma radiation, this being a weak evidence for an increasing abundance with admixture, probably driven by the increasing relative abundance of pentamethyldisilylmethyl. Therefore, it is not shown in Figure 9.

Water attachment to pentamethyldisilylmethyl forms species detected at 163, 181, and 199 amu. Interestingly, water attachment to the HMDS ion seems to be less effective than attachment to pentamethyldisilylmethyl, as discussed in Section 6. It has to be mentioned here, that the relative abundances of these ions do not decrease with increasing admixture but resemble approximately the abundance trend of the base ion. This could either mean, that the decreasing trend of the species associated with water attachment to trimethylsilyl is actually connected with a decrease of the trimethylsilyl density (see Section 4.3.2) or that additional unidentified ions contribute to the signals at these masses.

4.3.5 | Influence of capillary material

A puzzling feature of the mass spectra are the peaks around 102, 171, and 200 amu, which can not be explained by HMDS chemistry even including the common impurities. The relative abundances at these masses increase strongly with increasing admixture. However, this relative increase is only due to the decrease of the overall signal (see Figure 3), while the absolute signals of these species stays within a factor of 3–4. This indicates, that the source of the species leading to these signals is not connected with the precursor but with an untypical impurity, possibly coming from the plasma.

In a test measurement, we swapped the normally used borosilicate capillary with a quartz capillary (Friedrich & Dimmock, Inc.) and observed a strong decrease of the relative abundances of these species. The impact of the change of the capillary material can be seen in Figure 10 for admixtures of 100 ppm (respective upper figures) and 2000 ppm (respective lower figures) HMDS to argon. The identified species are marked again as in Figure 4. Due to the limited availability of quartz capillaries with square cross-sections, we used a slightly larger capillary than in the previous experiments. The inner cross-section of the quartz capillary is 1 by 1 mm, so no changes to the part housing the horizontal gas channel were necessary. The wall thickness was, however, 0.5 mm, leading to an electrode gap of 2 mm instead of the 1.4 mm of the borosilicate capillary. Due to this difference, the generator power needed for stable plasma operation increased and measurements were taken at 25 W instead of 10 W because of the larger voltage amplitude needed and with that larger power losses as well. Changes in the absolute number of ions due to different powers deposited in the plasma are corrected for by comparing only the relative abundances. The basic photochemistry is unaltered by the change of the capillary material, as the $HMDS^+$ ion is still dominant at both admixtures with 0.75 and 0.63 at 100 and 2000 ppm, respectively.

The results suggest that the formation of the vanishing species may be connected with species extracted from the capillary material by the plasma and that they are transported into the mass spectrometer in the same way as argon ions. The borosilicate capillary consists of 13% B_2O_3, 4% $N_2O + K_2O$ as well as 2.4% Al_2O_3 based on the data provided by the manufacturer. The Al_2O_3 molecule can be generated by laser vaporization of solid alumina and has a mass of 102 amu as well as an ionization potential of 8.9 eV, which is only slightly higher than that of HMDS.[87] This may be an explanation for the comparably high relative abundance of this species in the ion mass spectra. If B_2O_3 with 69 amu attaches to $Al_2O_3^+$, an ion with 171 amu could be formed. As both of these species are expected to be from the plasma region, either of them could be ionized. In case of the argon plasma photons, downstream ionization of B_2O_3 by the radiation is not possible (ionization potential 13.3 eV[88]), which explains the lower relative abundance of the ion at 171 amu when compared with the abundance with helium plasma photons. A similar explanation for the formation of the species at 100 and 101 amu as well as 200 amu is unfortunately not possible. Water and argon attachment to the species at 102 amu also takes place and is responsible for the peaks around 120 and 142 amu, as confirmed by the vanishing abundance in experiments with the quartz capillary.

The influence of the plasma effluent on the chemistry can be assessed by a modified source design, that inverts the plasma gas flow direction. A respective source is currently under development.

5 | CONCLUSION

We introduced a source of VUV-radiation, that is based on an atmospheric pressure plasma jet in pure argon and helium and which generates helium or argon excimer photons with wavelengths below the cut-off wavelength of typical VUV-windows. The possibility to use both gases enhances the versatility of the source, as the wavelength region of the VUV radiation can be selected based on the application. The so-called Capillary-Photon-Jet was then used to initiate photochemistry in 100–2000 ppm HMDS diluted in argon or helium for thin film deposition on silicon-wafers, which were subsequently analyzed by FTIR spectroscopy. FTIR spectra show that the deposits are strongly oxidized at low admixtures where the ratio of impurities to HMDS is higher and the VUV photons are not fully absorbed by the precursor and can interact with the substrate during deposition. Incorporation of oxygen from impurities takes place during deposition either in the gas phase or at active sites on the surface. At higher admixtures, the proportion of impurities in the deposited films decreases and the relative carbon content increases.

Additionally, the photochemistry has been studied by positive ion mass spectrometry to assess the main precursors for film formation. The chemistry taking place after precursor ionization is dominated by the $HMDS^+$ ion and further enhanced by water, oxygen and some unidentified impurities possibly connected with the capillary material. The main observed positive HMDS fragment ions include trimethylsilyl, pentamethyldisilanyl and pentamethyldisilylmethyl from breaking of the

Si–Si bond, Si–C, and C–H bond, respectively. We found only weak evidence for gas phase reactions of fragments among each other as the density of species produced by photodissociation is orders of magnitude lower than the density of neutral HMDS molecules in the irradiated region. The total ion flux from the source strongly decreases with admixture, as ions need to travel a longer distance to the sampling orifice in this case. As expected, the overall number of species increases when switching from the argon to the helium plasma radiation, as impurities can be ionized with the larger available photon energy and therefore contribute to the measured ions. A change of the capillary material from borosilicate to quartz led to a strong decrease of the relative abundances of several species that are not associated with HMDS photochemistry, indicating a production of these species in the plasma and a possibly turbulent transport to the sampling orifice.

AUTHOR CONTRIBUTIONS

Tristan Winzer: Investigation; formal analysis; visualization; writing–original draft. **Jan Benedikt**: Conceptualization; methodology; writing–review and editing; funding acquisition; project administration.

ACKNOWLEDGMENTS

Michael Poser, Volker Rohwer and Frank Brach are gratefully acknowledged for technical support. This research was funded by the German Research Association (DFG) in the project *Cold atmospheric plasmas for material synthesis: generation of silicon quantum dots and particle-free thin film deposition* (BE 4349/7-1). Open Access funding enabled and organized by Projekt DEAL.

DATA AVAILABILITY STATEMENT

The data that support the findings of this study are available from the corresponding author upon reasonable request.

ORCID

Tristan Winzer http://orcid.org/0000-0002-3834-9123
Jan Benedikt http://orcid.org/0000-0002-8954-1908

REFERENCES

[1] A. Grill, *J. Vac. Sci. Technol. B* **2016**, *34*(2), 020801.
[2] M. Gebhard, F. Mitschker, C. Hoppe, M. Aghaee, D. Rogalla, M. Creatore, G. Grundmeier, P. Awakowicz, A. Devi, *Plasma Process. Polym.* **2018**, *15*(5).
[3] H. Anma, Y. Yoshimoto, M. Warashina, Y. Hatanaka, *Appl. Surf. Sci.* **2001**, *175–176*, 484.
[4] D. A. Anderson, W. E. Spear, *Philos. Mag.* **1977**, *35*(1), 1.
[5] J. Saraie, Y. Fujii, M. Yoshimoto, K. Yamazoe, H. Matsunami, *Thin Solid Films* **1984**, *117*(1), 59.
[6] D.R. McKenzie, G. B., Smith Z. Q., Liu, *Phys. Rev. B: Condens. Matter* **1988**, *37*(15), 8875.
[7] H. Matsunami, T. Kimoto, *Mater. Sci. Eng. R Rep.* **1997**, *20*(3), 125.
[8] J. Z. Dávalos, T. Baer, *J. Phys. Chemff. A* **2006**, *110*(27), 8572.
[9] K. Takahashi, S. Nishino, J. Saraie, *J. Electrochem. Soc.* **1992**, *139*(12), 3565.
[10] H.-T. Chiu, J.-S. Hsu, *Thin Solid Films* **1994**, *252*(1), 13.
[11] N. Nordell, S. Nishino, J.-W. Yang, C. Jacob, P. Pirouz, *Appl. Phys. Lett.* **1994**, *64*(13), 1647.
[12] N. Nordell, S. Nishino, J.-W. Yang, C. Jacob, P. Pirouz, *J. Electrochem. Soc.* **1995**, *142*(2), 565.
[13] Y. J. Shi, X. Li, L. Tong, R. Toukabri, B. D. Eustergerling, *Phys. Chem. Chem. Phys.* **2008**, *10*(18), 2543.
[14] T. Takeuchi, M. Tanaka, T. Matsutani, M. Kiuchi, *Surf. Coat. Technol.* **2002**, *158–159*, 408.
[15] S. Yoshimura, S. Sugimoto, K. Murai, M. Kiuchi, *AIP Adv.* **2016**, *6*(12), 125029.
[16] S. Yoshimura, S. Sugimoto, T. Takeuchi, K. Murai, M. Kiuchi, *Nucl. Instrum. Methods Phys. Res. Sect. B* **2018**, *420*, 6.
[17] N. Inagaki, S. Kondo, M. Hirata, H. Urushibata, *J. Appl. Polym. Sci.* **1985**, *30*, 3385.
[18] J. L. C. Fonseca, J. P. S. Badyal, *Macromolecules* **1992**, *25*, 4730.
[19] J. L. C. Fonseca, D. C. Apperley, J. P. S. Badyal, *Chem. Mater.* **1992**, *4*, 1271.
[20] N. Shirtcliffe, P. Thiemann, M. Stratmann, G. Grundmeier, *Surf. Coat. Technol.* **2001**, *142–144*, 1121.
[21] T. Fujimoto, K. Okuyama, M. Shimada, Y. Fujishige, M. Adachi, I. Matsui, *J. Appl. Phys.* **2000**, *88*(5), 3047.
[22] M. C. M. van de Sanden, R. J. Severens, J. W. A. M. Gielen, R. M. J. Paffen, D. C. Schram, *Plasma Sources Sci. Technol.* **1996**, *5*, 268.
[23] W. M. M. Kessels, C. M. Leewis, M. C. M. van de Sanden, D. C. Schram, *J. Appl. Phys.* **1999**, *86*(7), 4029.
[24] W. M. M. Kessels, M. C. M. van de Sanden, D. C. Schram, *J. Vac. Sci. Technol. A* **2000**, *18*(5), 2153.
[25] A. de Graaf, M. F. A. M. van Hest, M. C. M. van de Sanden, K. G. Y. Letourneur, D. C. Schram, *Appl. Phys. Lett.* **1999**, *74* (20), 2927.
[26] J. Benedikt, M. Wisse, R. V. Woen, R. Engeln, M. C. M. van de Sanden, *J. Appl. Phys.* **2003**, *94*(10), 6932.
[27] J. Benedikt, S. Agarwal, D. Eijkman, W. Vandamme, M. Creatore, M. C. M. van de Sanden, *J. Vac. Sci. Technol. A* **2005**, *23*(5), 1400.
[28] J. Benedikt, D. Eijkman, W. Vandamme, S. Agarwal, M. C. M. van de Sanden, *Chem. Phys. Lett.* **2005**, *402*(1–3), 37.
[29] J. Benedikt, D. C. Schram, M. C. M. van de Sanden, *J. Phys. Chem. A* **2005**, *109*(44), 10153.
[30] J. Perrin, O. Leroy, M. C. Bordage, *Contrib. Plasma Phys.* **1996**, *36*(1), 3.
[31] O. May, J. Fedor, B. C. Ibănescu, M. Allan, *Phys. Rev. A* **2008**, *77*(4), 040701.
[32] S. Wickramanayaka, Y. Hatanaka, Y. Nakanishi, A. M. Wróbel, *J. Electrochem. Soc.* **1994**, *141*(10), 2910.
[33] A. M. Wróbel, S. Wickramanayaka, Y. Nakanishi, Y. Hatanaka, S. Pawłowski, W. Olejniczak, *Diam. Relat. Mater.* **1997**, *6*(9), 1081.

[34] S. Wickramanayaka, A. M. Wróbel, Y. Hatanaka, *Hyomen Kagaku* **1997**, *18*(2), 108.
[35] Y.-Y. Xu, T. Muramatsu, T. Aoki, Y. Nakanishi, Y. Hatanaka, *MRS Proc.* **1998**, *544*, 185.
[36] A. M. Wróbel, A. Walkiewicz-Pietrzykowska, M. Stasiak, T. Aoki, Y. Hatanaka, J. Szumilewicz, *J. Electrochem. Soc.* **1998**, *145*(3), 1060.
[37] Y. Hatanaka, K. Sano, T. Aoki, A. M. Wróbel, *Thin Solid Films* **2000**, *368*(2), 287.
[38] Y.-Y. Xu, T. Muramatsu, M. Taniyama, T. Aoki, Y. Hatanaka, *Thin Solid Films* **2000**, *368*(2), 181.
[39] A. M. Wróbel, S. Wickramanayaka, K. Kitamura, Y. Nakanishi, Y. Hatanaka, *Chem. Vap. Depos.* **2000**, *6*(6), 315.
[40] A. M. Wróbel, A. Walkiewicz-Pietrzykowska, Y. Hatanaka, S. Wickramanayaka, Y. Nakanishi, *Chem. Mater.* **2001**, *13*(5), 1884.
[41] A. M. Wróbel, A. Walkiewicz-Pietrzykowska, J. E. Klemberg-Sapieha, Y. Hatanaka, T. Aoki, Y. Nakanishi, *J. Appl. Polym. Sci.* **2002**, *86*, 1445.
[42] S. A. Starostin, M. Creatore, J. B. Bouwstra, M. C. M. van de Sanden, H. W. de Vries, *Plasma Process. Polym.* **2015**, *12*(6), 545.
[43] F. Massines, C. Sarra-Bournet, F. Fanelli, N. Naudé, N. Gherardi, *Plasma Process. Polym.* **2012**, *9*(11–12), 1041.
[44] M. Miettinen, M. Johansson, S. Suvanto, J. Riikonen, U. Tapper, T. T. Pakkanen, V.-P. Lehto, J. Jokiniemi, A. Lähde, *J. Nanopart. Res.* **2011**, *13*(10), 4631.
[45] V. Raballand, J. Benedikt, A. von Keudell, *Appl. Phys. Lett.* **2008**, *92*, 091502.
[46] V. Raballand, J. Benedikt, S. Hoffmann, M. Zimmermann, A. von Keudell, *J. Appl. Phys.* **2009**, *105*, 083304.
[47] L. Bröcker, G. S. Perlick, C. -P. Klages, *Plasma Process. Polym.* **2020**, *17*(11), 2000129.
[48] S. K. Tokach, R. D. Koob, *J. Phys. Chem.* **1980**, *84*(1), 1.
[49] T. Brix, E. Bastian, P. Potzinger, *J. Photochem. Photobiol. A Chem.* **1989**, *49*, 287.
[50] R. K. Wells, J. P. S. Badyal, *Macromolecules* **1993**, *26*, 3187.
[51] P. Kurunczi, J. Lopez, H. Shah, K. H. Becker, *Int. J. Mass Spectrom.* **2001**, *205*1–3, 277.
[52] J. Golda, B. Biskup, V. Layes, T. Winzer, J. Benedikt, *Plasma Process. Polym.* **2020**, *56*, 1.
[53] S. Schneider, F. Jarzina, J.-W. Lackmann, J. Golda, V. Layes, V. Schulz-von der Gathen, J. E. Bandow, J. Benedikt, *J. Phys. D Appl. Phys.* **2015**, *48*(44), 444001.
[54] T. Winzer, D. Steuer, S. Schüttler, N. Blosczyk, J. Benedikt, J. Golda, *J. Appl. Phys.* **2022**, *132*(18), 183301.
[55] T. Trickl, E. F. Cromwell, Y. T. Lee, A. H. Kung, *J. Chem. Phys.* **1989**, *91*(10), 6006.
[56] R. G. Tonkyn, J. W. Winniczek, M. G. White, *Chem. Phys. Lett.* **1989**, *164*(2–3), 137.
[57] R. H. Page, R. J. Larkin, Y. R. Shen, Y. T. Lee, *J. Chem. Phys.* **1988**, *88*(4), 2249.
[58] I. M. T. Davidson, P. Potzinger, B. Reimann, *Ber. Bunsenges. Phys. Chem.* **1982**, *86*(1), 13.
[59] R. Ellul, P. Potzinger, B. Reimann, *J. Phys. Chem.* **1984**, *88*(13), 2793.
[60] S. Takagi, M. Ishikawa, M. Kumada, K. Takayoshi, F. Ryoichi, *Thermochim. Acta* **1986**, *109*, 55.
[61] S. Große-Kreul, S. Hübner, S. Schneider, D. Ellerweg, A. von Keudell, S. Matejčík, J. Benedikt, *Plasma Sources Sci. Technol.* **2015**, *24*(4), 044008.
[62] J. Benedikt, A. Hecimovic, D. Ellerweg, A. von Keudell, *J. Phys. D Appl. Phys.* **2012**, *45*(40), 403001.
[63] Y. Harada, J. N. Murrell, H. H. Sheena, *Chem. Phys. Lett.* **1968**, *1*(12), 595.
[64] H. Hoffmeyer, P. Potzinger, B. Reimann, *J. Phys. Chem.* **1985**, *89*(22), 4829.
[65] M. Jaritz, H. Behm, C. Hopmann, D. Kirchheim, F. Mitschker, P. Awakowicz, R. Dahlmann, *J. Phys. D Appl. Phys.* **2017**, *50*(1), 015201.
[66] I. M. T. Davidson, I. L. Stephenson, *J. Chem. Soc. A* **1968**, 282.
[67] L. Szepes, T. Baer, *J. Am. Chem. Soc.* **1984**, *106*(2), 273.
[68] K. Shiina, M. Kumada, *J. Org. Chem.* **1958**, *23.1*, 139.
[69] H. Sakurai, R. Koh, A. Hosomi, M. Kumada, *Bull. Chem. Soc. Jpn* **1966**, *39*(9), 2050.
[70] H. Sakurai, A. Hosomi, M. Kumada, *Chem. Commun.* **1968**, (16), 930.
[71] C. Eaborn, J. M. Simmie, *Chem. Commun.* **1968**, (22), 1426.
[72] I. M. T. Davidson, A. B. Howard, *J. Chem. Soc. Chem. Commun.* **1973**, (9), 323.
[73] I. M. T. Davidson, C. Eaborn, J. M. Simmie, *J. Chem. Soc. Faraday Trans. 1* **1974**, *70*(0)249.
[74] I. M. T. Davidson, A. B. Howard, *J. Chem. Soc. Faraday Trans. 1* **1975**, *71*(0), 69.
[75] S. Patzer, N. L. Arthur, P. Potzinger, H. G. Wagner, *J. Photochem. Photobiol. A Chem.* **1997**, *110*, 221.
[76] X. Liu, J. Zhang, A. Vazquez, D. Wang, S. Li, *J. Phys. Chem. A* **2019**, *123*, 10520.
[77] L. E. Gusel'nikov, N. S. Nametkin, V. M. Vdovin, *Acc. Chem. Res.* **1975**, *8*(1), 18.
[78] P. Potzinger, A. Ritter, J. Krause, *Z. Naturforsch. A* **1975**, *30*(3)347.
[79] J. E. Baggott, M. A. Blitz, H. M. Frey, P. D. Lightfoot, R. Walsh, *Chem. Phys. Lett.* **1987**, *135*(1–2), 39.
[80] X. M. Li, B. D. Eustergerling, Y. J. Shi, *Int. J. Mass Spectrom.* **2007**, *263*(2–3), 233.
[81] A. C. M. Wojtyniak, J. A. Stone, *Int. J. Mass Spectrom. Ion Processes* **1986**, *74*(1), 59.
[82] M. C. Flowers, L. E. Gusel'nikov, *J. Chem. Soc. B: Phys. Org.* **1968**, 419.
[83] S. K. Tokach, R. D. Koob, *J. Am. Chem. Soc.* **1980**, *102*(1), 376.
[84] J. L. Jauberteau, I. Jauberteau, *J. Phys. Chem. A* **2012**, *116*(35)8840.
[85] J. Berkowitz, G. B. Ellison, D. Gutman, *J. Phys. Chem.* **1994**, *98*(11), 2744.
[86] I. M. T. Davidson, *J. Organomet. Chem.* **1988**, *341*(1–3), 255.
[87] S. B. H. Bach, S. W. McElvany, *J. Phys. Chem.* **1991**, *95*(23), 9091.
[88] M. Asano, T. Kou, *J. Chem. Thermodyn.* **1988**, *20*(10), 1149.

How to cite this article: T. Winzer, J. Benedikt, *Plasma. Process. Polym.* **2024**, e2300226. https://doi.org/10.1002/ppap.202300226